Revealing the Cu^{2+} ions localization at low symmetry Bi sites in photorefractive $Bi_{12}GeO_{20}$ crystals doped with Cu and V by high frequency EPR

Revealing the Cu^{2+} ions localization at low symmetry Bi sites in photorefractive $Bi_{12}GeO_{20}$ crystals doped with Cu and V by high frequency EPR

Sergiu V. Nistor[a*], Mariana Stefan[a], Etienne Goovaerts[b], François Ramaz[c], Bernard Briat[c1]

[a] *National Institute of Materials Physics, POB MG 7, 077125 Magurele, Romania*

[b] *Physics Department - CDE, University of Antwerp, Universiteitsplein 1, 2610 Antwerpn (Wilrijk), Belgium*

[c] *Institut Langevin, Ondes et Images, ESPCI ParisTech, PSL Research University, CNRS UMR 7587, INSERM U979, Université Paris VI – Pierre et Marie Curie, 1 rue Jussieu, 75005 Paris, France*

Abstract

The sites of incorporation of Cu^{2+} impurity ions in $Bi_{12}GeO_{20}$ single crystals co-doped with copper and vanadium have been investigated by electron paramagnetic resonance (EPR). While the X-band EPR spectra consist of a simple broad ($\Delta B \sim 50$ mT) line with anisotropic lineshape, the W-band EPR spectra exhibit well resolved, strongly anisotropic lines, due to transitions within the $3d^9$ - ^2D ground manifold of the Cu^{2+} ions. The most intense group of lines, attributed to the dominant Cu^{2+}(I) center, displays a characteristic four components hyperfine structure for magnetic field orientations close to a <110> direction. The $\boldsymbol{g}$ and $\boldsymbol{A}$ tensor main axes are very close to one of the 12 possible sets of orthogonal <1-10>, <00-1> and <110> crystal directions. Several less intense lines, with unresolved hyperfine structure and similar symmetry properties, mostly overlapped by the Cu^{2+}(I) spectrum, were attributed to Cu^{2+}(II) centers. The two paramagnetic centers are identified as substitutional Cu^{2+} ions at Bi^{3+} sites with low C_1 symmetry, attributed to different configurations of neighboring charge compensating defects.

Keywords: high frequency EPR, $Bi_{12}GeO_{20}$, Cu^{2+}

[*]Corresponding author. *E-mail address*: snistor@infim.ro (S. V. Nistor)
[1]Retired. *E-mail address*: briat.bernard@wanadoo.fr (B. Briat)

1. Introduction

The study of point defects and impurity ions in $Bi_{12}MO_{20}$ (M = Si, Ge, Ti) crystals with sillenite structure is essential for understanding their role in the generation and transfer of photoinduced charge carriers responsible for the photochromic and photorefractive effects in these materials [1,2].

Optical absorption (OA), magnetic circular dichroism (MCD), optical detection of magnetic resonance (ODMR) and electron magnetic resonance (EMR) studies [3-7] have proven the assumption [6] that Bi_M^{4+} paramagnetic point defects, which consist of a hole trapped at the oxygen neighbors of the tetrahedrally coordinated Bi^{3+} ion substituting for a M^{4+} ion in one of the MO_4 tetrahedra (Bi_M^{3+} + h), are responsible for the photorefractive properties of nominally pure $Bi_{12}MO_{20}$ crystals.

The role of various impurity cations in the photorefractive properties of crystalline $Bi_{12}MO_{20}$ has been also investigated by various spectroscopy methods [8-14]. Of special interest are the impurity paramagnetic transition metal ions (TMIs) such as: V^{4+}, Cr^{3+}, Mn^{2+}/ Mn^{4+}, Fe^{3+}, Co^{2+}, Cu^{2+}, which can be investigated by magneto-optical and EMR techniques.

The presently investigated $Bi_{12}GeO_{20}$ (abbreviated BGO) exhibits an unit cell (cubic space group I23) with lattice constant a = 1.01455 nm [15]. It contains geometrically regular oxygen tetrahedra, centered on a Ge^{4+} ion (Figure 1a), as well as Bi^{3+} ions sevenfold coordinated by five oxygen atoms at distances ranging from 0.2076 nm (1a), through 0.2220 nm (1b), 0.2228 nm (2), 0.2623 nm (1c) to 0.2640 nm (3), forming an incomplete octahedron, plus two oxygen atoms situated at 0.3082 nm (1d) and 0.3170 nm (1e), as shown in Figure 1b. Compared to the Ge^{4+} ions localized at lattice sites with cubic (T_d) symmetry and Ge-O distance of 0.1717 nm, the incomplete octahedral arrangement, with all different Bi-O distances, results in a low C_1 symmetry of the Bi^{3+} site. There are two possible substitutional localizations of the impurities, at the high T_d symmetry Ge^{4+} site and at the low C_1 symmetry Bi^{3+} site [15]. The different local symmetry properties at the two cationic sites are expected to result in electron paramagnetic resonance (EPR) spectra reflecting the localization of the substitutional paramagnetic impurities.

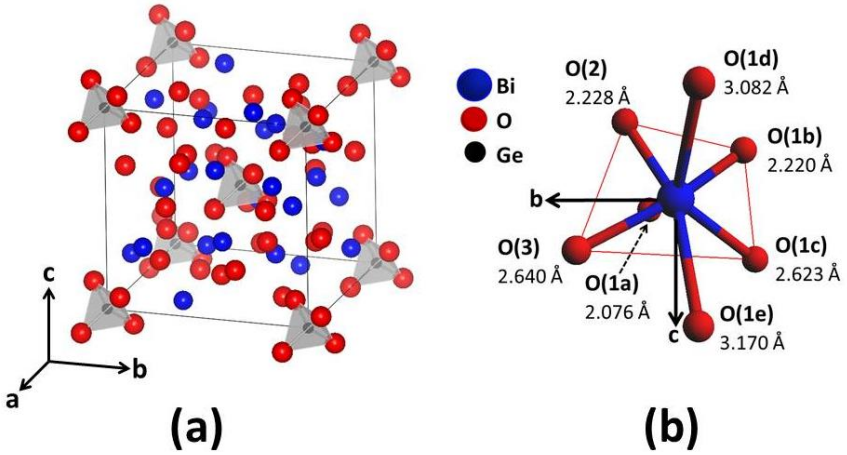

Figure 1. Structure of the sillenite $Bi_{12}GeO_{20}$ (BGO) illustrated by: (a) the unit cell with the shaded regular tetrahedrons of O^{2-} ligands surrounding each Ge^{4+} cation, (b) one of the Bi^{3+} cations with the seven nearest neighbor O^{2-} ligands, represented in the reference frame of the Oabc crystal axes, viewed along the a axis. The ligand notations correspond to data from ref. [15]). (2-column fitting image)

According to the symmetry properties of the observed spectra, the TMIs so-far investigated in BGO by EPR, namely Fe^{3+} [16,17], Mn^{2+} [18] and Cr^{4+} [19,20], were found to be localized at the tetrahedrally coordinated Ge^{4+} sites. This is somewhat surprising considering the difference between the ionic radii and/or charge state of the investigated impurity ions and the substituted Ge^{4+} ion. However, in $Bi_{12}SiO_{20}$ doped with ruthenium Ramaz et al. [13] reported the occurrence of Ru^{3+} and Ru^{5+} ions in the low symmetry Bi sites on the basis of correlated MCD and X-band EPR measurements.

Here we present the results of a multifrequency EPR investigation of the Cu^{2+} ions in BGO crystals heavily co-doped with copper and vanadium (BGO:CuV) [21]. The vanadium, which has been added in the melt in order to enhance the incorporation of copper into the BGO lattice, has been initially thought to be present as diamagnetic V_{Ge}^{5+} [21]. Later, in a combined optical/MCD/ODMR investigation of BGO crystals doubly doped (weakly) with vanadium and a second transition metal (Cr, Mn, Co, Cu), the presence of V, Cr and Mn in the 4+ charge state was concluded *via* ODMR in blue-illuminated samples [12]. Furthermore, the $^2E > {}^2T_2$ internal transition of V_{Ge}^{4+} was found in all MCD spectra.

The presence of paramagnetic $S = 1/2$ centers, attributed to Cu^{2+} ions at sites with axial symmetry, has been inferred in heavily doped BGO:CuV crystals by Chevrier et al. from a preliminary X-band EPR study [22]. We found from spectral simulations that the two sets

of axial *g*-components determined in ref. [22] from the simple analysis of the single crystal and powder spectra, respectively, could not accurately describe our experimental X-band spectra, especially those recorded at lower temperatures.

As will be shown here, the low temperature W-band (94 GHz) high frequency EPR measurements resulted in well-resolved spectra, allowing an accurate characterization of the individual paramagnetic centers present in the BGO:CuV crystal. The spin Hamiltonian (SH) analysis of the spectra recorded at $T \leq 20$ K on oriented single crystal specimens resulted in the identification of two Cu^{2+}-type centers with close parameters, both attributed to substitutional Cu^{2+} ions at Bi^{3+} sites with low C_1 symmetry, as reflected in the *g*-values and the occurrence of off-diagonal *g*-components. For the dominant center a four component hyperfine (hf) structure characteristic for the stable Cu^{2+} isotopes with $I = 3/2$ nuclear spin was resolved for field orientations close to <110>. The difference in the SH parameters of the two centers was tentatively attributed to the different surrounding possibly involving perturbing charge compensating defects.

2. Experimental

The investigated samples were cut from a Czochralski grown, orange colored $Bi_{12}GeO_{20}$ single crystal co-doped with copper and vanadium (BGO:CuV), with an initial concentration in the starting material corresponding to formula $Bi_{12}[Ge_{0.7}Cu_{0.1}V_{0.2}]O_{20}$ [21]. Due to strong segregation effects [6], the actual concentration of both doping ions in the resulting single crystal is expected to be much smaller. Samples for the present X (9.4 GHz) and W (94 GHz) band EPR measurements, of 2x2x3 mm^3 and 0.3x0.3x1.5mm^3 size respectively, with the long (rotation) axis along one of the <100> or <110> axes, were cut from a single crystal piece originating from the same single crystal boule which provided the samples for the X-band EPR investigations reported in ref. [22].

The continuous-wave EPR measurements were performed on standard spectrometers from Bruker, models ESP300E and ELEXSYS E600, operating in the X- and W-band, respectively, equipped with gas-flow cryogenic systems for investigations in the 3.6–300 K temperature range. To avoid microwave saturation effects the measurements were performed at $T \geq 10$ K. The high magnetic field required for the W-band EPR measurements was provided by an Oxford Instruments 6T superconducting split-coil magnet on a rotating base.

The X-band samples were mounted in homemade holders, which did not obstruct the direct *in-situ* illumination of the samples and allowed a controlled rotation of the sample. The possibility to tilt the microwave cavity in a vertical plane allowed an accurate orientation of the specific crystal directions along the applied magnetic field.

The tiny W-band samples (Figure 2) were mounted under the optical microscope in the open end of sample holders consisting of pure fused silica tubes with 0.5 mm inner diameter filled with high vacuum grease, as described in ref. [23].

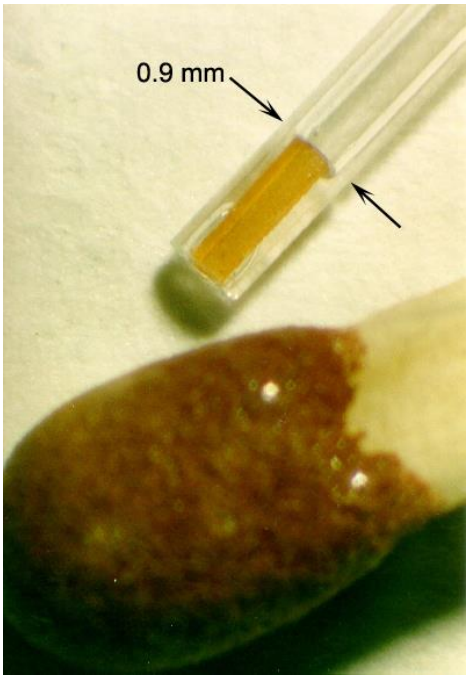

Figure 2. View of a BGO:CuV single crystal sample cut with the long axis parallel to a <110> crystalline direction, inserted in a W-band fused silica tube EPR sample holder, shown next to a match head to better illustrate its small size. (1 column fitting image)

A small tilting of the sample long (rotation) axis with respect to the corresponding <110> or <001> crystal directions resulted from cutti ng and polishing operations as well as from the mismatch between the sample and the inner diameter of the sample holder. In this case it was not possible to correct the vertical tilting of the microwave cavity containing the sample with respect to the EPR spectrometer magnetic field rotation axis. The tilting angles, representing the Euler angles between the reference frame with the sample rotation axis taken as a z-axis and the cubic crystal axes, were determined from the analysis of the EPR spectra angular dependence with the EPRNMR v.6.4 (Department of Chemistry, University of Saskatchewan, Canada) program. Comparable values, of less than 3 degrees, varying from sample to sample, were found with an automated four circle X-ray

diffractometer, by directly mounting the sample holder with the BGO:CuV crystal inside on the goniometer head of the diffractometer.

The EPR measurements in both X- and W-bands were performed with the magnetic field vector rotated in the {110} and {001} crystal planes. The orientation of the magnetic field vector in the rotation plane with respect to the crystal main axes was obtained, within a few degrees accuracy, by optical alignment of one of the {110} or {100} polished facets parallel to the magnetic field. A more accurate alignment followed from optimization based on the anisotropy of the recorded spectra.

The analysis of the EPR spectra, including the determination of the SH parameters and the spectral lineshape analysis by simulation/deconvolution procedures, were performed with the computer programs EPRNMR v.6.4 and Easy Spin v.4.2 [24].

3. Results

3. 1. Low frequency X-band EPR measurements

X-band EPR measurements were performed on both oriented single crystals and a powder sample obtained by finely crushing a single crystal piece. The single crystal EPR spectra, which could be observed in the whole measuring temperature range (3.8 -295 K), consist of a broad, derivative-like line with anisotropic lineshape and a maximum width of ~50 mT (Figures 3a to 3c). The observed strong intensity increase with decreasing temperature, without important changes in the lineshape, is characteristic for transitions inside a ground doublet with a dominantly inhomogeneously broadened line. Small changes in the lineshape took place with the temperature decrease, down to 80 K, with no further changes at lower temperatures.

The changes in the EPR signal lineshape, observed by rotating the magnetic field in the {110} and {001} crystal planes of a BGO:CuV single crystal, were previously attributed [22] to the presence of an axial paramagnetic center with $S = 1/2$ and g-values $g_{\|} = 2.49$ and $g_{\perp} = 2.04$. However, as shown in Figure 3b, the angular dependence of the spectra seems to be better described, in a rough approximation, by the $g_{\|} = 2.30$ and $g_{\perp} = 2.04$ values attributed to the $S = 1/2$ center reported in the polycrystalline BGO:CuV used as starting material for the single crystal growth [22].

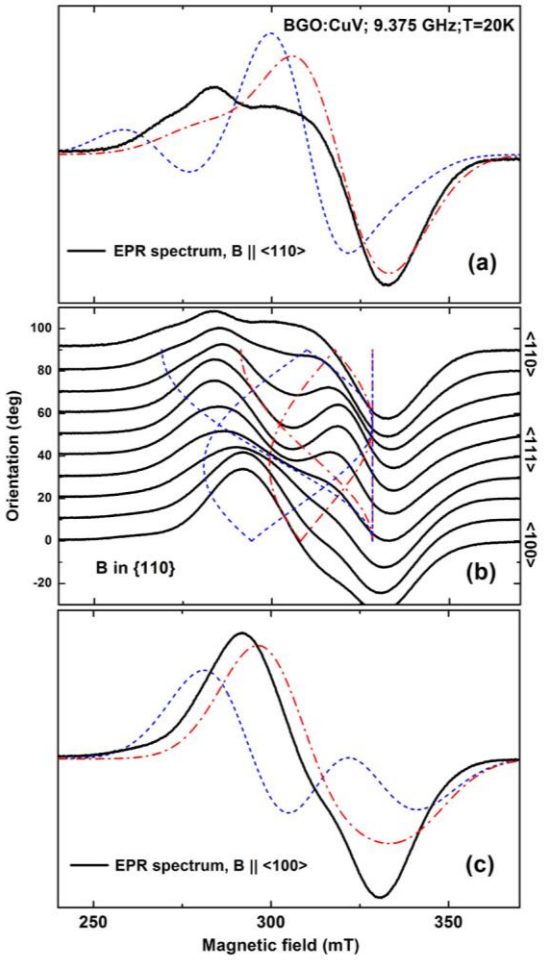

Figure 3. The X-band EPR spectra (continuous lines) of a BGO:CuV single crystal recorded at T = 20 K, with the magnetic field B: (a) || <110>, (b) rotated in a {110} plane in steps of 10 degrees, (c) || <100>. Simulations of the angular dependence and line shape for the axial S = 1/2 paramagnetic centers with parameters: $g_{\|}$ =2.49, $g_{\perp}$ = 2.04, ΔB_{pp} = 16.5 mT (short dash line) and $g_{\|}$ = 2.30, $g_{\perp}$ = 2.04, ΔB_{pp} = 24.5 mT (dash-dot line) are also presented. (1 column fitting image)

As illustrated in Figures 3a and 3c, it is not possible to obtain a good fitting of the experimental spectra with lineshape simulations based on the above mentioned axial g-values even when optimizing the linewidth values ΔB_{pp}. The EPR spectrum lineshape of the powdered BGO:CuV sample recorded at low temperature cannot be properly fitted with either of the two sets of previously reported [19] axial parameters as well (Figure 4), even after optimizing the linewidth values. It should be mentioned that it was not possible to satisfactorily simulate both single crystal and powder EPR spectra with a single rhombic S = 1/2 paramagnetic center either. The difficulties encountered in describing accurately

the experimental X-band EPR spectra of the single crystal and powder BGO:CuV with an axial or rhombic $S = 1/2$ paramagnetic Cu^{2+} center with isotropic linewidth suggest a more

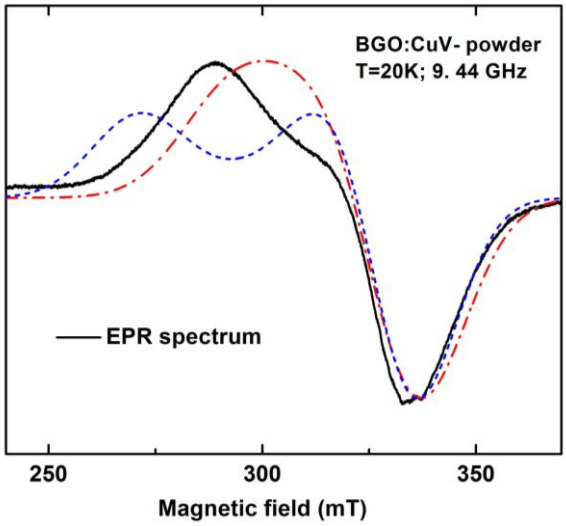

Figure 4. The powder X-band EPR spectrum of a finely crushed BGO:CuV crystal, recorded at T = 20 K (continuous line) and the lineshape simulations for the axial $S = 1/2$ centers with the same parameters and notations as in Figure 3. (1 column fitting image)

complex situation. Thus, one could consider a more general anisotropic lineshape for the Cu^{2+} centers, very likely associated with the hf structure from the two naturally occurring ^{63}Cu (69.09%) and ^{65}Cu (30.91%) isotopes, both with $I = 3/2$ nuclear spin and close nuclear moments ($^{65}\mu / {}^{63}\mu = 1.07$) and/or the presence of two or more types of Cu^{2+} centers with different SH parameters.

To understand this situation we decided to perform high frequency W (94 GHz)-band EPR investigations, which allowed us to observe the individual spectra lines of the Cu^{2+} paramagnetic centers and determine their SH parameters.

3. 2. The high frequency W-band EPR measurements

The resulting W-band EPR spectra recorded at T ≤ 20 K consist of several separate, strongly anisotropic lines (Figures 5). The most intense group of lines is attributed to the so-called Cu^{2+}(I) center, responsible for the observed EPR spectra. The angular dependence of the Cu^{2+}(I) center line positions for the magnetic field rotated in the {100} and {110} crystal planes suggests a basic orthorhombic symmetry, with local axes parallel to one of the 12 equivalent sets of orthogonal crystal directions x || [1-10], y || [00-1] and z || [110]. The lowest magnetic field line of this spectrum for B || <110>

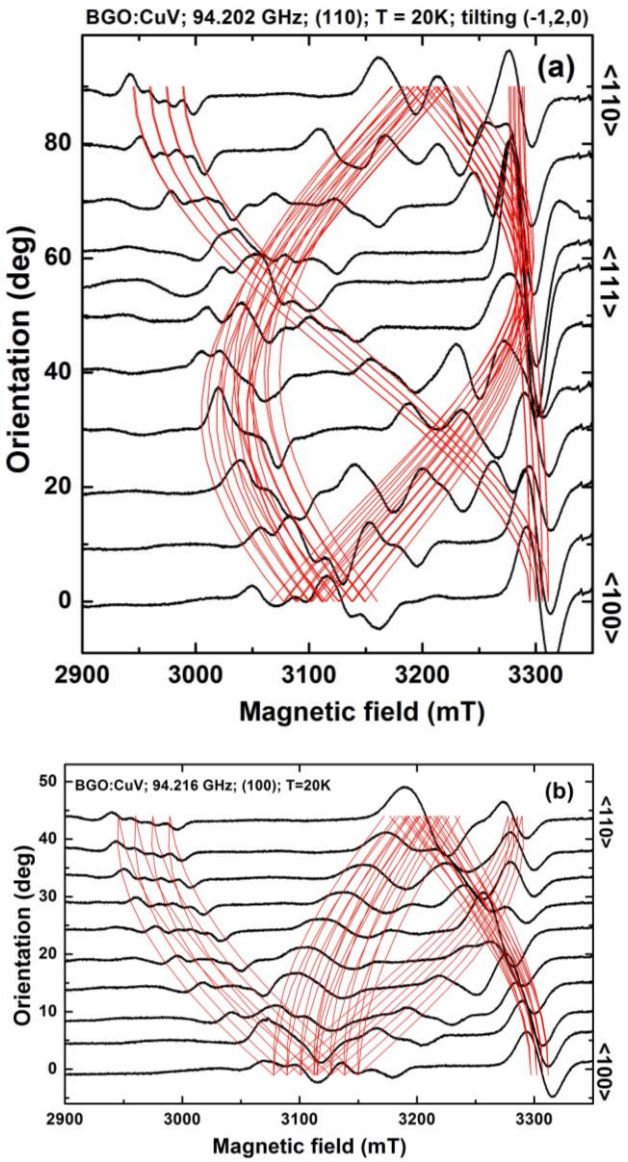

Figure 5. W-band EPR spectra of a BGO:CuV single crystal recorded at T = 20 K, for magnetic field rotated in steps of 10 degrees: (a) in a {110} plane, and (b) in a {100} plane. The angular dependence of the line positions calculated with the spin Hamiltonian parameters of the Cu^{2+}(I) center reported in Table 1, including the tilting angle (if present) is are superposed. (1 column fitting image)

exhibits a four components hf structure (Figure 6a), confirming that a single Cu^{2+} ion is involved in the defects responsible for the observed spectra. Indeed, copper is the only impurity element present in our crystals in a significant concentration, with I = 3/2 nuclear spin from the two ^{63}Cu and ^{65}Cu isotopes with 100% total abundance. Orthorhombic local symmetry of the Cu^{2+}(I) centers would require that at most four separate lines were present

in the spectrum for orientations of the magnetic field in the {110} or {100} planes, away from the main crystalline axes. However, the spectra presented in Figures 5 exhibit for many orientations up to six lines. The observed splitting of the symmetry degenerate lines can be explained by a rotation of the local axes of the Cu^{2+}(I) center away from the nominal crystal directions. In the spin-Hamiltonian formalism this rotation can be taken into account by including non-zero off-diagonal *g*-components. We found that the angular dependence of the lines attributed to the Cu^{2+}(I) centers with ^2D ($3d^9$) ground state is described by the spin Hamiltonian with usual [25] notations :

$$H = g_{xx}\beta B_x S_x + g_{yy}\beta B_y S_y + g_{zz}\beta B_z S_z + g_{xz}\beta(B_x S_z + B_z S_x) + g_{yz}\beta(B_y S_z + B_z S_x) + \\ + A_{xx} S_x I_x + A_{yy} S_y I_y + A_{zz} S_z I_z \quad (1)$$

Here $S = 1/2$, $I = 3/2$ and the reference frame of both $\boldsymbol{g}$ and $\boldsymbol{A}$ tensors correspond to one of the 12 possible sets of orthogonal <1-10>, <00-1> and <110> crystal directions. Only the nonzero $\boldsymbol{g}$-tensor components are included here. For the $\boldsymbol{A}$ tensor, the experimental resolution is insufficient to discern low symmetry effects and only the diagonal elements are included. In determining the SH parameters we took into account the eventual small tilting with up to a few degrees of the BGO:CuV samples with respect to the rotation axis, an effect that could be minimized by choosing the best oriented samples from the analysis of the spectra angular dependence.

The SH parameters of the Cu^{2+}(I) centers were determined according to the following procedure. Average *g*-values were initially obtained from the line positions (or the center of the hf multiplet) in the spectra recorded for the magnetic field along the main <100>, <111> and <110> crystal axes. Further on, the resulting values were used as input data to determine both the diagonal elements of the hf interaction tensor $\boldsymbol{A}$ and to improve the *g*-parameters by fitting the calculated spectral lineshape to the experimental spectra recorded for the <100>, <111> and <110> magnetic field orientations. Finally, the resulting SH parameter values were checked with the recorded angular dependences in both {110} and {100} planes, as shown in Figures 5. The resulting SH parameters are given in Table 1.

Table 1. The spin Hamiltonian parameters of the Cu^{2+} centers in BGO:CuV expressed in the reference frame x || [1-10], y || [00-1], z || [110] (one of the 12 equivalent orientations of the center)

Center/ host	g_{xx}	g_{yy}	g_{zz}	off-diagonal g_{ij}	A_x **(mT)**	A_y **(mT)**	A_z **(mT)**	**Note**
Cu^{2+}(I) / $B_{12}GeO_{20}$	2.0500 ± 0.0007	2.0377 ± 0.0007	2.2684 ± 0.0005	g_{xz} = 0.013 ± 0.002 g_{yz} = 0.003 ± 0.001	4.0 ± 0.5	5.0 ± 0.5	16.5 ± 0.3	(a)
Cu^{2+}(II) / $B_{12}GeO_{20}$	2.050 ± 0.005	2.038 ± 0.005	2.315 ± 0.003	g_{xz} = 0.018 ± 0.003 g_{yz} = 0.003 ± 0.002	-	-	-	(b)

(a) Based on W-band EPR spectra at T = 20 K. $(\Delta B_{pp})^{hf}$ = 15.5 ± 0.5 mT. The *A* components represent average values for the two natural Cu isotopes. Diagonal g_X = 2.0492; g_Y = 2.0377, g_Z = 2.2692 components correspond to the principal axis system (X,Y,Z) with eigenvectors: X(0.9981;-0.0153;-0.0590), Y(0.0146;0.9998;-0.0138), Z(0.0592;0.0129;0.9982).

(b) Approximate values, resulting from the W-band spectra at T = 10K. No hf interaction data are available. Diagonal g_X = 2.049; g_Y = 2.038, g_Z = 2. 316 components correspond to the principal axis system (X,Y,Z) with eigenvectors: X(0.9976;-0.0187;-0.0673), Y(0.0179;0.9998;-0.0120), Z(0.0674;0.0108;0.9977).

The determination of the SH parameters was subject to errors due to several factors. Thus, because of the broad lines (derivative peak to peak linewidth $\Delta B_{pp} \leq 60$ mT), with a more or less resolved hf structure, it was difficult to obtain spectra corresponding to accurate orientations, within less than ±1 degree from the <100> and <110> crystal axes. This was further complicated by the presence of the small tilting of the samples, resulting in additional line splitting. Although this effect has been considered in the fitting procedures, it still left us without a perfect fit of the lineshape of all EPR transitions along the <100> and <111> directions. Another source of errors was the overlap with a second set of less intense lines from the so-called Cu^{2+}(II) centers. Considering all these aspects, the angular dependence of the line positions calculated with the SH parameters given in Table 1 fits in a satisfactory manner the experimental data (see Figures 5). One should

mention that the hf parameters and the individual linewidth $(\Delta B_{pp})^{hf}$ = 15.5 mT of the hf components have been estimated from lineshape simulations and comparison with the experimental results (Figures 6).

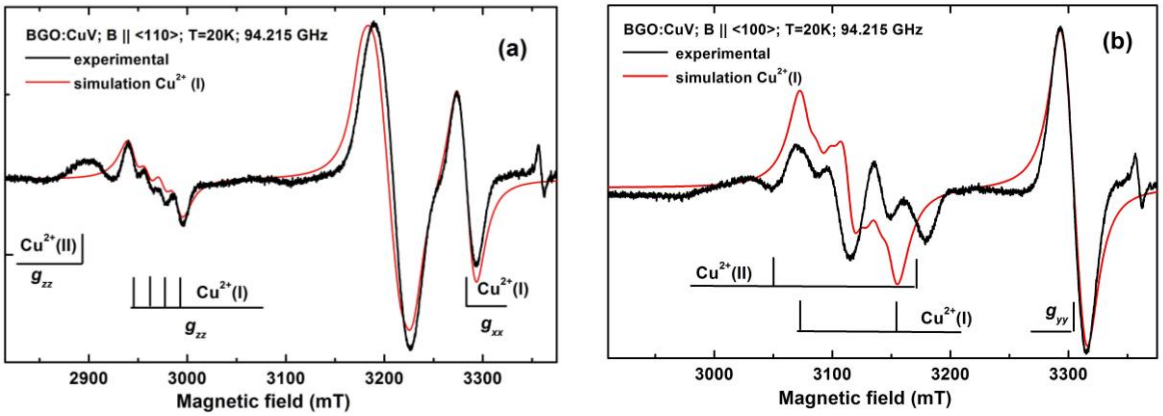

Figure 6. The W-band EPR spectra of a BGO:CuV single crystal sample recorded at T = 20 K for : (a) B || <110>, and (b) B || <100> orientations. Experimental spectra (thick lines) and lineshape simulations (thin lines) of the Cu^{2+}(I) centers with the SH parameters given in Table 1. Line position of the Cu^{2+}(II) centers are also mentioned. The sharp signal at g ~ 2 is due the central ΔM = + ½ to- ½ transition from traces of Fe^{3+} ions localized at the cubic Ge^{4+} sites [16]. (2 columns fitting image)

Due to the presence of a resolved hf structure just for B || <110>, one could accurately determine only the A_{zz} hf component. Consequently the other two hf components A_{xx} and A_{yy} could be estimated with less accuracy from the lineshape simulations, considering the broad structureless line to result from the convolution of four equidistant lines of the same intensity, assuming their individual linewidth to be isotropic. Moreover, due to the large $(\Delta B_{pp})^{hf}$ = 15.5 mT value, the resulting hf parameters represent an average value for the two Cu isotopes. One should also mention that the presence of non-diagonal hf interaction terms in the SH (1) cannot be entirely excluded.

A pair of additional, less intense EPR lines, partly overlapped by the more intense Cu^{2+}(I) centers lines, shadowing on the lower magnetic field side the g_{zz} - component line of the Cu^{2+}(I) centers, are better seen at T = 10 K for rotations of the magnetic field in a {001} plane (Figure 7). These lines, which do not exhibit a resolved hf structure, are attributed to a second center, denoted Cu^{2+}(II).

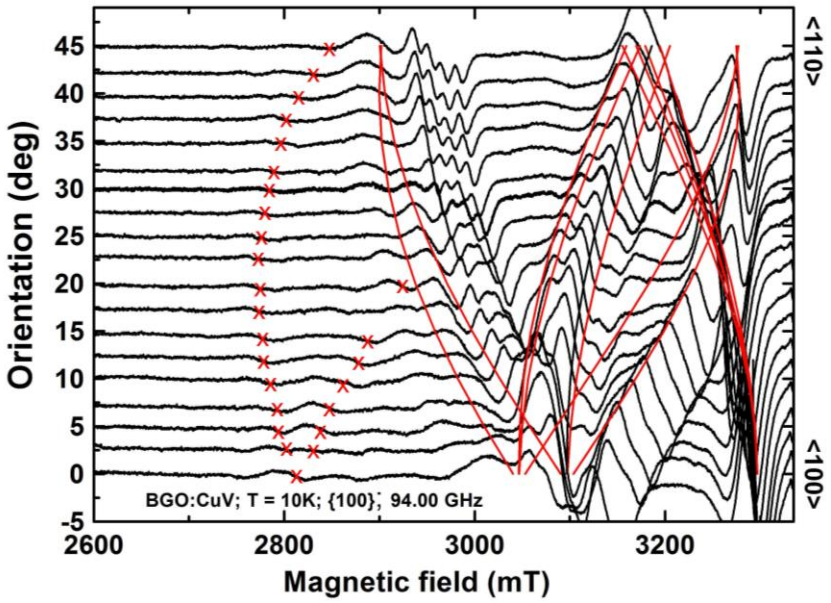

Figure 7. The W-band EPR spectra at T = 10 K for magnetic field rotated in a {100} plane in steps of 5 degrees magnified for a better view of the lines attributed to the Cu^{2+}(II) centers. Their angular dependence calculated with the SH parameters given in Table 1 is superposed. Additional less intense lines from unidentified anisotropic centers with larger *g*-components are marked by crosses. The sample tilting is slightly different from that of the sample presented in Figure 4b . (1 column fitting image)

For B || <110> the two lines are degenerate (Figure 6a), resulting in a line with effective g_{zz} = 2.31 value and an estimated linewidth ΔB_{pp} = 55 mT, comparable to the overall ΔB_{pp} = 53 mT value of the adjacent g_{zz} – composite line of the Cu^{2+}(I) centers. A careful examination of the spectra recorded in the {100} plane (Figure 7) shows that the component lines from the Cu^{2+}(II) centers with other local orientations are partly, or even completely hidden under the more intense lines of the Cu^{2+}(I) center. Therefore one expects close g_{xx} and g_{yy} values for the two Cu^{2+} centers. For the Cu^{2+}(II) centers one can also estimate an off-diagonal g_{xz} = 0.018 value by fitting the splitting observed upon rotation in the {001} plane. Figure 7 exhibits the angular dependence of the line positions (without hf splitting) in the {001} plane for the Cu^{2+}(II) centers, calculated with the SH parameters presented in Table 1, superposed on the experimental spectra. The overall fitting of line positions and shapes is improved after the inclusion of a small off-diagonal component g_{yz} = 0.003. In spite of the remaining discrepancies in the low field component of the Cu^{2+}(I) spectrum for B || <100> (Figure 6b), the overall fitting is satisfactory. The

rather close values of the *g*-parameters for the two observed Cu^{2+} centers suggest similar structural models, in both cases involving a Cu^{2+} ion substituting for a Bi^{3+} ion. The difference seems to arise from the presence of a perturbing charge compensating defect in one of the two centers, or else in both, but in different configurations.

The presence of the two Cu^{2+} centers with different SH parameters and anisotropic linewidth, resulting from the hf interaction anisotropy, not to mention other centers, possibly associated with Cu^{2+} ions responsible for the less intense lines with larger *g*-values, marked with crosses in the spectra recorded at T = 10 K (Figure 7), can explain the difficulties encountered in the analysis of the X-band EPR spectra. Accurate lineshape simulations of the X-band EPR spectra, even using the SH parameters of the Cu^{2+} centers obtained from the analysis of the W-band EPR spectra, are still difficult to perform, as they involve the unknown frequency dependent change in the linewidth. Moreover, while the X-band EPR lineshape is best described by a Gaussian, the W-band lineshape is close to Lorentzian, which means that the dominant mechanism of line broadening changes with the frequency.

4. Discussion

The multifrequency EPR investigations of the doubly doped BGO:CuV crystals have revealed the presence of two types of paramagnetic Cu^{2+} centers with distorted local orthorhombic symmetry. The dominant Cu^{2+}(I) center, with the main axes of both ***g*** and ***A***-tensors close to one of the 12 possible sets of orthogonal <1-10>, <00-1> and <110> crystal directions, has been identified and characterized by the analysis of the high frequency W-band EPR spectra. An accurate fitting of both line positions and spectra lineshape along the main crystal directions required non-zero off-diagonal g_{xz} and g_{yz} components, expected to occur for Cu^{2+} ions localized at lattice sites with very low symmetry [26,27].

Another group of less intense lines, with similar local symmetry, partly overlapped by the lines of the Cu^{2+}(I) centers, has been attributed to the Cu^{2+}(II) center. This spectrum exhibits a larger g_{zz} = 2. 315 value, similar g_{xx} and g_{yy} values, but different off-diagonal g_{xz} and g_{yz} components. Due to the overlap from the more intense lines of the Cu^{2+}(I) centers it was impossible to follow precisely the angular variation of the other lines from the Cu^{2+}(II) centers and to determine accurate *g*-parameters. The overlap of the Cu^{2+}(I) and Cu^{2+}(II) spectra together with the strong linewidth anisotropy from unresolved hf interactions explain, why all the attempts to simulate the X-band EPR spectral lineshape with a single

axial or orthorhombic $S = 1/2$ spectrum with isotropic lineshape were unsuccessful. One should mention that in the absence of complete sets of hypefine tensor components the diagonalization of the SH (1) had to be limited to the g-components. The small changes in the resulting diagonal g-components given in the footnotes of Table 1, reflect the small angles between the xyz reference frame and the XYZ principal axes directions, as can be easily seen from the reported values of the rotation matrices.

Despite all our efforts we have not been able to identify any EPR transitions which could be attributed to the paramagnetic vanadium ions V^{4+} or V^{3+}. Such centers are expected to give EPR transitions with effective $g < 2$ values. In the case of the non-Kramers V^{3+} ions with $3d^2$ configuration, the EPR detection is quite problematic, because of either large ZFS, or a large spread in the ZFS parameter leading to broadening of the resonances [25]. In the case of V^{4+} ions ODMR experiments at 1.4 K in the Q band [28] have shown that the MCD signal (assigned to V_{Ge}^{4+} with $g = 1.86$) at e.g. 650 nm and 700 nm is practically fully quenched at resonance, i.e. the EPR signal is saturated. A similar result was reported in the case of V-doped $Bi_4Ge_3O_{12}$ [29]. These results suggest that V^{4+} ions could be difficult to detect because of easy saturation and a narrow T-region for EPR measurements.

The analysis of the EPR data offers an insight into the problem of determining the localization sites of the Cu^{2+} ions in the BGO lattice. Two possible lattice sites should be *a priori* taken into consideration, namely the four-fold coordinated Ge^{4+} site at the center of a regular tetrahedron of oxygen ligands (Figure 2a) and the low symmetry Bi^{3+} site coordinated by seven oxygen ligands with different bond lengths and orientations, of which the five closest ones form an incomplete octahedral arrangement (Figure 1b).

Although quite unlikely in view of the larger ionic radius of Cu^{2+} (0.071 nm) compared to Ge^{4+} (0.053 nm) ions and the large difference in the electrical charge, we shall firstly consider the Ge^{4+} site occupancy by a Cu^{2+} ion. One possibility would be the presence, for charge compensation reasons, of an oxygen vacancy in one of the four nearest neighbor oxygen ligand sites, resulting in a local crystal field with <111> trigonal symmetry, a situation which was not observed experimentally. In the case of charge compensation at distance, one expects the orbital degeneracy of the lowest $^2T_2$ triplet state from the ^2D (d^9) free ion state of a Cu^{2+} ion in a crystal field with tetrahedral T_d symmetry to be lifted by the Jahn-Teller (JT) effect, resulting in a local distortion with either trigonal <111> or tetragonal <100> symmetry [30,31]. In both cases the ground state wave function would consist mainly of contributions from the |xy>, |xz> and |yz> free ion 3*d* wave functions.

None of these local distortions was observed in the case of two Cu^{2+} centers. Although not observed by EPR, a relatively small amount of Cu^{2+} seems to be also present at the Ge^{4+} site in our crystals by the occurrence of relatively sharp absorption and MCD [11] features in the 5500-6500 cm^{-1} spectral range. Actually, it is possible that tetrahedrally localized Cu^{2+} ions are responsible for the weak anisotropic lines at low magnetic fields, corresponding to $g > 2.31$, marked by crosses in the spectra recorded at T = 10 K (Figure 7).

The substitution of the Bi^{3+} ions by Cu^{2+} ions is more likely considering the smaller ionic radius of the Cu^{2+} ions (0.087 nm) compared to the ionic radius of the Bi^{3+} ions (0.117 nm) in a seven fold coordination and the smaller difference in the charge states. Such substitution can also explain the results of the W-band EPR spectra analysis. Indeed, considering the local crystal field at the Bi^{3+} site as resulting in the first approximation from a six-fold coordination with the closer oxygen ions (see Figure 1b) one expects the orbital degeneracy of the lowest ^2E orbital doublet from the ^2D (d^9) free ion state of a Cu^{2+} ion in a crystal field with octahedral symmetry to be lifted by the existing low symmetry local crystal field. In such a case the two resulting orbital states would be based on the $|x^2 - y^2>$ or $|3z^2 - r^2>$ free ion 3*d* wave functions [32]. Examining the resulting *g* values for either the Cu^{2+}(I) or Cu^{2+}(II) center one finds that in a quasi-axial approximation ($g_x \cong g_y \cong g_\perp$) the *g*-values fulfill the relationships $g_\parallel = g_e + 8\lambda/\Delta_0 > g_\perp = g_e + 2\lambda/\Delta_1 > 2$, which correspond to a $|x^2 - y^2>$ ground state, with usual notations [32]. One should mention that in such localization the broad EPR spectra lines of the two Cu^{2+} centers can be explained by the presence of unresolved SH interactions with the large nuclear moment of the ^{209}Bi nuclei (I = 9/2; 100 % abundance) from the neighbouring Bi^{3+} ligands situated at distances comparable to the longer Bi-O bonds [15].

We emphasize that in the BGO:CuV host lattice the low symmetry *g*-tensor of the Cu^{2+} ions reflects the intrinsic low symmetry of the substituted Bi^{3+} site.

Finally, one should consider a possible interstitial localization of the Cu^{2+} ions in the BGO lattice. Such localization has been investigated by optical absorption in the case of chromium ions in BGO crystals [20]. Uniaxial stress measurements indicated the occurrence in this case of interstitial sites with orthorhombic symmetry, a situation different from the present BGO:CuV case, where the local symmetry is lower.

Early investigations have shown [9] that by adding Cu^{2+} impurity ions the photorefractivity of the BGO:CuV crystals increased. To determine the involvement of the

presently identified Cu^{2+} centers in the reported photorefractivity we investigated their photosensitivity by monitoring the photo induced changes in the EPR spectrum. The photosensitivity of the Cu^{2+} centers was determined by "in situ" illumination of the BGO:CuV samples in the X-band EPR spectrometer, at T = 20 K. Experiments were performed with the magnetic field oriented along the <100>, <110> and <111> directions, using the narrow band light from a 100 W xenon lamp and an appropriate combination of lenses, cut-off and interference filters. The experiments were performed under ambient red (670 nm) light (which according to early tests did not influence the EPR spectrum), by excitation with blue (λ_m = 455 nm) and yellow (λ_m = 562 nm) light, at T = 60 K and 20 K, for periods of up to 30 minutes. The rather small variation (~5%) in the amplitude of the EPR spectrum, observed in these measurements, should be considered in relation with the large absorption coefficient at these wavelengths [12,28]. As a result only a small fraction of the investigated crystal is effectively illuminated and participates in the photochromic effect, which means that the photo induced effect in the whole sample is much larger. It is therefore possible that the observed Cu^{2+} centers are involved in the reported photorefractivity increase [9].

5. Conclusions

The EPR investigation of oriented samples cut from a BGO:CuV single crystal resulted in the identification of two types of Cu^{2+} centers with low symmetry properties, attributed to the substitutional localization of the Cu^{2+} ions at the Bi^{3+} low symmetry C_1 lattice site. The minor differences in the orientation of the local main axes for the two centers, resulting from the different off-diagonal *g*-component values, as well as the small difference in the g_{zz}-values, point to very similar defect structures. One center may be formed by simple Bi^{3+} to Cu^{2+} substitution, while the second would involve a neighboring perturbing (and eventually charge compensating) defect. However, it is not excluded that both centers are perturbed by defects in two different configurations. The nature of the perturbing defects could not be determined here, but might be explored via electron nuclear double resonance (ENDOR) measurements. Such measurements could also be fruitful in determining the role of vanadium ions in the incorporation and localization of the Cu^{2+} ions.

These results strongly suggest that the simple model of an activating impurity ion substitutionally localized at a certain lattice cation site, usually employed in the analysis of

photorefractivity, should be replaced by a more complex model with the activating impurity ions localized at two or more sites involving neighboring lattice defects.

Acknowledgments

The present work has been performed in the frame of a scientific cooperation between the National Institute of Materials Physics (NIMP), Magurele, Romania and the University of Antwerp, Belgium, which also involved a collaboration with former Laboratoire d'Optique Physique – ESPCI Paris, France. Financial support from ANCSI Romania (CEEX M3 no.63/2006 and CORE PN06-410103 projects) and the Fund for Scientific Research (FWO; group project G.0116.06N) - Flanders is kindly acknowledged. Upgrade investments of the Antwerp EPR instrumentation was provided by the Hercules Foundation of Flanders, Belgium (contract AUHA013). The authors would like to express their gratitude to L. Rossou from EMAT-UA laboratory for the laborious preparation of the samples for the W-band EPR measurements. Our thanks go also to J.C. Launay (Bordeaux) for providing us with the BGO:CuV crystals.

References

[1] B. Briat, V.G. Grachev, G.I. Malovichko, O.F. Schirmer, M. Wöhlecke, in: P. Gunther and J. P. Huignard (Eds.), Photorefractive Materials and Their Applications, Springer Verlag, Berlin, 2007, Vol. 2, pp 9-49; ISBN 978-0-387-34081-4.

[2] A. F. Lima, M. V. Lalic, First-principles study of the Bi_MO_4 antisite defect in the $Bi_{12}MO_{20}$ (M=Si, Ge, Ti) sillenite compounds, J. Phys.: Condens. Matter. 25 (2013) 495505 1-9. doi:10.1088/0953-8984/25/49/495505

[3] B. Briat, C. L. Boudy**,** J. C. Launay, Magnetic and natural circular dichroism of $Bi_{12}GeO_{20}$: Evidence for several paramagnetic centres, Ferroelectrics 125 **(**1992**)** 467-469. doi:10.1080/00150199208017112

[4] H. J. Reyher, U. Hellwig, O. Thiemann, Optically detected magnetic resonance of the bismuth-on-metal-site intrinsic defect in photorefractive sillenite crystals, Phys. Rev. B 47 (1993) 5638-5645. doi:10.1103/PhysRevB.47.5638

[5] B. Briat, H. J. Reyher, A. Hamri, N. G. Romanov, J. C. Launay, F. Ramaz, Magnetic circular dichroism and the optical detection of magnetic resonance for the Bi antisite defect in $Bi_{12}GeO_{20}$, J. Phys.: Condens. Matter. 7 (1995) 6951-6959. doi:10.1088/0953-8984/7/34/017

[6] B. C. Grabmaier, R. Oberschmid, Properties of Pure and Doped $Bi_{12}GeO_{2o}$and $Bi_{12}SiO_{20}$ Crystals, phys. stat. sol. (a) 96 (1986) 199-210. doi: 10.1002/pssa.2210960124

[7] I. Ahmad, V. Marinova, E. Goovaerts, High-frequency electron paramagnetic resonance of the hole-trapped antisite bismuth center in photorefractive bismuth sillenite crystals, Phys. Rev. B 79 (2009) 033107 1-4. doi: 10.1103/PhysRevB.79.033107

[8] M.T. Borowiec, Photochromic absorption of $Bi_{12}GeO_{20}$ doped with copper, Phys. B 132 (1985) 223-231. doi:10.1016/0378-4363(85)90068-3

[9] N. Wolffer, P. Gravey, J. Y. Moisan, C. Laulan, J. C. Launay, Analysis of double phase conjugate mirror interaction in absorbing photorefractive crystals: Application to BGO:Cu, Opt. Commun. 73 (1989) 351-356. doi:10.1016/0030-4018(89)90170-3

[10] B. Briat, V. Topa, C. Laulan Boudy, J. C. Launay, Sites and valencies of chromium in bismuth germanates: a magnetic circular dichroism and absorption study, J. Lumin. 53 (1992) 524-528. doi:10.1016/0022-2313(92)90214-T

[11] B. Briat, A. Hamri, F. Ramaz, H. Bou Rjeily, Magnetooptical characterization of ligand field bands and charge transfer processes in sillenite oxides, XII Conf. on Solid State Cryst. Mater. Sci. and Appl., Oct. 7-11, 1996, Zakopane, Poland, in: SPIE Proc., 3178 (1997) 160-168.

[12] B. Briat, M.T. Borowiec, H. Bou Rjeily, F. Ramaz, A.Hamri**,** H. Szymczak, Combined Optical/MCD/ODMR investigations of photochromism in doubly-doped Bi_{12} GeO_{20}, Rad. Eff. Def. Sol. 157 (2002) 989-993. doi:10.1080/10420150215806

[13] F. Ramaz, L. Rakitina, M. Gospodinov, B. Briat, Photorefractive and photochromic properties of ruthenium-doped Bi12SiO20, Opt.Mater. 27 (2005) 1547-1559. doi:10.1016/j.optmat.2004.11.007

[14] V. Marinova, I. Ahmad, E. Goovaerts, Photoinduced absorption study of carrier dynamics in Ru-doped Bi12SiO20 crystals after nanosecond laser pulse excitation, J. Appl. Phys. 107 (2010) 113106 1-7. doi: 10.1063/1.3418443

[15] S. C. Abrahams, P. B. Jamieson, J. L. Bernstein, Crystal Structure of Piezoelectric Bismuth Germanium Oxide $Bi_{12}GeO_{20}$, J. Chem. Phys. 47 (1967) 4034-4041. doi:10.1063/1.1701572

[16] W. Wardzynski, M. Baran, H. Szymczak, Electron paramagnetic resonance of Fe^{3+} in bismuth germanium oxide single crystals, Phys. B 111 (1981) 47-50. doi:10.1016/0378-4363(81)90163-7

[17] S. I. Goloshchadov, L. B. Kuleva, E. I. Leonov, V. M. Orlov, E. B. Shadrin, ESR of Fe^{3+} in BSO, BGO, BTO and $Bi_{25}FeO_{40}$. Inorg. Mater. 22 (1986) 770-772.

[18] W. Wardzynski, H. Szymczak, M. T. Borowiek, K. Pataj, T. Lukasiewicz, J. Zmija, Light-induced charge transfer processes in Mn-doped $Bi_{12}GeO_{20}$ and $Bi_{12}SiO_{20}$ single crystals, J. Phys. Chem. Sol. 46 (1985) 1117-1129. doi:10.1016/0022-3697(85)90140-4

[19] W. Wardzynski, H. Szymczak, K. Pataj, T. Lukasiewicz, J. Zmija, Light induced charge transfer processes in Cr doped $Bi_{12}GeO_{20}$ and $Bi_{12}SiO_{20}$ single crystals, J. Phys. Chem. Sol. 43 (1982) 767-769. doi:10.1016/0022-3697(82)90242-6

[20] W. Wardzynski, H. Szymczak, The center of orthorhombic symmetry in chromium doped $Bi_{12}GeO_{20}$ and $Bi_{12}SiO_{20}$ single crystals, J. Phys. Chem. Sol. 45 (1984) 887-896. doi:10.1016/0022-3697(84)90129-X

[21] J. P. Fontaine, G. P. Extremet, V. Chevrier, J. C. Launay, Experimental and theoretical treatments of the Czochralski growth of $Bi_{12}GeO_{20}$, J. Cryst. Growth 139 (1994) 67-80. doi:10.1016/0022-0248(94)90029-9

[22] V. Chevrier, J. M. Dance, J. C. Launay, R. Berger, Cu^{2+} in $Bi_{12}GeO_{20}$: a tentative electron spin resonance study, J. Mater. Sci. Lett. 15 (1996) 363-365.

[23] S. V. Nistor, M. Stefan, E. Goovaerts, A. Bouwen, D. Schoemaker, G. Dinca, Point defects in cubic boron nitride crystals, Diam. Rel. Mat. 10 (2001) 1408-1411. doi:10.1016/S0925-9635(00)00396-4

[24] S. Stoll, A. Schweiger, EasySpin, a comprehensive software package for spectral simulation and analysis in EPR, J. Magn. Reson. 178 (2006) 42-55. doi:10.1016/j.jmr.2005.08.013

[25] J. R. Pilbrow, Transition Ions Electron Paramagnetic Resonance, Clarendon Press, Oxford, 1991.

[26] D. G. McGavin, Symmetry constrains on EPR spin Hamiltonian parameters, J. Magn. Res. 74 (1987) 19-55.

[27] C. Rudowicz, P. Gnutek, Modeling techniques for analysis and interpretation of electron magnetic resonance (EMR) data for transition ions at low symmetry sites in crystals—A primer for experimentalists, Phys. B 404 (2009) 3582-3593. doi:10.1016/j.physb.2009.06.060

[28] B. Briat, F. Ramaz, unpublished results.

[29] B. Briat, A. Watterich, F. Ramaz, L. Kovacs, B.C. Forget, N. Romanov, Charge states and optical transitions of vanadium in $Bi_4Ge_3O_{12}$ identified by MCD and ODMR, Opt. Mater. 20 (2002) 253-262. doi:10.1016/S0925-3467(02)00066-6

[30] C. A. Bates, P. E. Chandler, The Jahn-Teller interaction and $3d^9$ ions at tetrahedral sites, J. Phys. C: Sol. State. 4 (1971) 2713-2724. doi:10.1088/0022-3719/4/16/036

[31] C. A. Bates, P. E. Chandler, The Jahn-Teller interaction and $3d^9$ ions at tetrahedral sites. II. Tetragonal distortions, J. Phys. C: Sol. State. 6 (1973) 1975-1980. doi:10.1088/0022-3719/6/11/023

[32] A. Abragam and B. Bleaney, Electron Paramagnetic Resonance of Transition Ions, Clarendon, Oxford 1970.

Graphical abstract